ChemComm

COMMUNICATION

View Article Online
View Journal | View Issue

Cite this: *Chem. Commun.*, 2025, **61**, 9972

Received 29th April 2025,
Accepted 28th May 2025

DOI: 10.1039/d5cc02417j

rsc.li/chemcomm

Syntheses and characterisation of terephthalonitrile radical salts†

Meng-Ting Suo,[a] Jouke A. Fleege,[a] Nathan J. Yutronkie,[ab] Vincent L. Nadurata,[a] Dmitry Chernyshov,[b] Mathieu Rouzières,[a] Aaron Mailman,[c] Rodolphe Clérac *[a] and Pierre Dechambenoit *[a]

Two terephthalonitrile radical salts have been synthesized, isolated and characterized as $Li^+(tpn)^{\bullet-}(THF)_2$ and $Na^+(tpn)^{\bullet-}(THF)$ (tpn = terephthalonitrile; THF = tetrahydrofuran). Single crystal X-ray diffraction reveals that the lithium and sodium ions are bridged by $tpn^{\bullet-}$ and further coordinated by THF solvent molecules, forming 1-D and 3-D coordination networks, respectively. While the lithium salt exhibits paramagnetic behaviour, the sodium analogue is diamagnetic in the solid state due to strong π–π interactions between tightly stacked $tpn^{\bullet-}$ pairs. These readily isolable radical salts are versatile precursors for cross-coupling reactions and mild organic reductants, and could be used as attractive ligands for designing high temperature molecular magnets and conductive materials.

The design of molecule-based conductive materials and/or room temperature magnets requires the use of molecular components that enable a large delocalization of the charge and/or the spin.[1–3] Using organic radicals as bridging ligands in coordination polymers is strongly attractive in this context,[4–8] especially if the unpaired electron is fully delocalized on a π system with significant d–π orbital overlap.[9–12] In particular, organonitrile radicals were found to be efficient magnetic relays for making high temperature molecule-based magnets such as $V[TCNE]_x{\cdot}yCH_2Cl_2$ ($x \approx 2, y \approx 1/2$) (TCNE = tetracyanoethylene; T_c = 400 K),[13] or could promote electrical conductivity in solids, as in [TCNQ][TTF][14] or [TCNA][TTF][15] (TCNQ = tetracyanoquinodimethane, TCNA = tetracyanoazulene, TTF = tetrathiafulvalene). Other interests of organonitrile radicals reside in the good predictability of their self-assembly through linear coordination modes, and the stabilization of their radical redox states owing to the electron-withdrawing cyanide groups.

One of the simplest organonitriles is 1,4-benzenedicarbonitrile, also referred as 1,4-dicyanobenzene or terephthalonitrile (tpn). This versatile reagent has been reported to be redox active and can be reduced to either a persistent radical-anion ($tpn^{\bullet-}$)[16–18] or dianion (tpn^{2-}).[19] Interestingly, DFT calculations have shown that the unpaired electron in $tpn^{\bullet-}$ is delocalized across the entire molecule,[18,20] making it an excellent linker for the design of high temperature magnets and conductors. Additionally, it recently gained attention as a precursor or intermediate for electrochemical cross-coupling reactions[21–24] and reductions.[16,17] However, $tpn^{\bullet-}$ has typically been generated *in situ* without isolation,[21–24] or only poorly characterized.[25–27] We report here the straightforward syntheses of $Li^+(tpn)^{\bullet-}(THF)_2$ and $Na^+(tpn)^{\bullet-}(THF)$ (THF = tetrahydrofuran) along with their structural, spectroscopic and magnetic characterizations.

Both alkali salts can be prepared by a dropwise addition of THF solutions of lithium or sodium 1,2-dihydroacenaphthylenide[28] into a colorless solution of tpn in dry THF. Alternatively, they can be prepared by a stoichiometric reaction of tpn with the corresponding alkali metal (see ESI†). Upon addition, olive-green crystals of $Li^+(tpn)^{\bullet-}(THF)_2$ precipitate immediately, while the more soluble $Na^+(tpn)^{\bullet-}(THF)$ was obtained by subsequent addition of dry diethyl ether (see ESI;† solubilities in THF: 0.6 g L^{-1} *vs.* 1.1 g L^{-1}).

In solution, the radical exhibits stability in dry THF. Cyclic voltammetry of tpn in THF reveals two reversible reductions at −2.25 and −3.16 V *vs.* Fc^+/Fc (Fig. S3, ESI†). Each of these processes involves a one-electron transfer, indicating that the radical is fairly stable with a comproportionation constant of $\sim 2.5 \times 10^{15}$. This is further corroborated by EPR of both solutions (Fig. S4, bottom, ESI†), which give *g* values of 2.0025 and 2.0037, respectively. UV-vis spectra of the dark solutions of the lithium and sodium salts in THF display intense absorption bands at 397 and 431 nm characteristic of π–π* transitions in organonitrile radicals (Fig. S5, ESI†).[29]

[a] *Univ. Bordeaux, CNRS, CRPP, UMR 5031, F-33600 Pessac, France. E-mail: pierre.dechambenoit@u-bordeaux.fr, rodolphe.clerac@u-bordeaux.fr*
[b] *ESRF—The European Synchrotron, 38043 Grenoble, France*
[c] *University of Jyväskylä, Department of Chemistry, Nanoscience Centre, P.O. Box 35, FI-40014 Jyväskylä, Finland*

† Electronic supplementary information (ESI) available: Experimental and synthetic methods, crystallographic and spectroscopic data, and additional magnetic data. CCDC 2350103–2351405. For ESI and crystallographic data in CIF or other electronic format see DOI: https://doi.org/10.1039/d5cc02417j

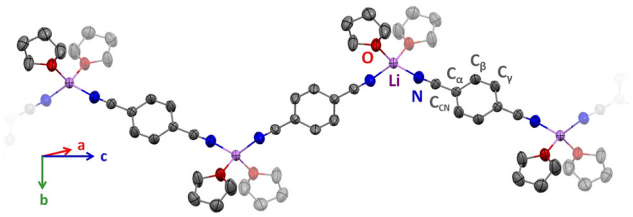

Fig. 1 Portion of the crystal structure of $Li^+(tpn)^{\bullet-}(THF)_2$ at 250 K, showing the 1-D coordination network. Thermal ellipsoids are depicted at a 50% probability level. Hydrogen atoms are omitted for clarity.

Single crystals were successfully isolated directly from THF solution or by vapor diffusion of diethyl ether (Fig. S1 and S2, ESI†), allowing the crystalline solids to be characterised by powder- and single-crystal X-ray diffraction. Both compounds crystallize in the monoclinic *C*2/*c* space group.

At 250 K, $Li^+(tpn)^{\bullet-}(THF)_2$ forms a one-dimensional (1-D) coordination polymer with radical anions bridging lithium cations. Each Li^+ center adopts a tetrahedral geometry, coordinated by two THF oxygen atoms (d(Li···O) = 1.942(5) Å) and two nitrile nitrogens (d(Li···N) = 1.999(5) Å) from $tpn^{\bullet-}$ forming corrugated chains, as illustrated in Fig. 1. These chains remain well-isolated in the crystal structure (Fig. 2, left).

Remarkably, cooling to 120 K results in a reversible phase change where the initially equivalent chains become three crystallographically distinct chains as depicted in blue, red, and green in the top part of Fig. 2. While the space group remains *C*2/*c*, the unit cell volume expands from 1641.7(7) $Å^3$ to 6257.4(6) $Å^3$. The interatomic distances within the three chains are similar (d(Li···N) = 1.974(6)–2.008(6)Å – Table 1). The phase

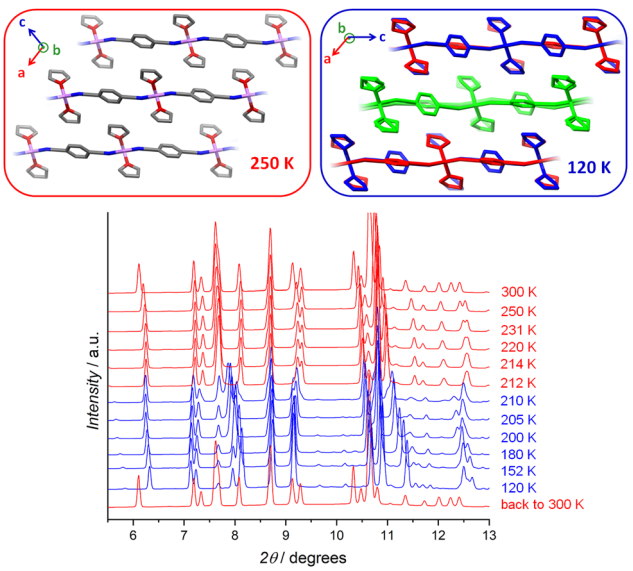

Fig. 2 Top left: stick representation of the packing of the chains in the crystal of $Li^+(tpn)^{\bullet-}(THF)_2$ at 250 K. Color code: C grey, N blue, O red, Li pink, and H atoms are omitted for clarity. Top right: stick representation of the packing of the three crystallographically independent chains at 120 K. Bottom: thermal evolution of the powder X-ray diffractograms between 300 and 120 K.

purity of the samples at both temperatures was checked by powder X-ray diffraction (Fig. S7, ESI†), and the reversibility of the structural phase transition was further evidenced by the thermal evolution of the diffractograms (Fig. 2 bottom and Fig. S9, ESI†).

Unlike the corrugated chains of $Li^+(tpn)^{\bullet-}(THF)_2$, the sodium analogue, $Na^+(tpn)^{\bullet-}(THF)$, self-assembles into a three-dimensional coordination network. This architecture results from the octahedral coordination of the Na ions bridged by bis-μ_2-tpn and terminal μ-THF ligands. The structure features linear arrays of sodium ions extending along the *c*-axis, with each Na^+ connected to its neighbors through one μ-THF and two bis-μ-bonded nitrile groups from the $tpn^{\bullet-}$ (Fig. 3 and Fig. S10, ESI†). The Na^+ ions adopt a distorted N_4O_2 octahedral geometry, with the oxygen atoms alternatively in *cis*- and *trans*-positions (d(Na···O) = 2.484(2)–2.490(2) Å) and d(Na···N) = 2.373(2)–2.4662(2) Å). Notably, the $tpn^{\bullet-}$ ligands form stacked pairs with an average interplanar spacing $d_{tpn-tpn}$ of 3.24 Å (Fig. 3), indicating significant π–π interactions between radicals.[30] Thus, the $tpn^{\bullet-}$ units serve dual roles, where they bridge sodium ions while engaging in radical–radical interactions.

Beyond the charge balance considerations, which supports the presence of tpn in its radical form, the analysis of the intramolecular bond distances is essential to further demonstrate the formal oxidation state and, more importantly, to gain further insights into the electronic rearrangement upon reduction. While the crystal structure of neutral tpn is well documented, we selected a high-resolution and low-temperature reference structure for reliable comparison[31] (Table 1). As expected, significant differences are observed when comparing bond distances for the neutral tpn and $tpn^{\bullet-}$ in the lithium and sodium salts. The nitrilic C≡N bond lengths increase only slightly, whereas the C_{CN}–C_α distances shorten significantly but are temperature-independent. Furthermore, the C_α–C_β distance in the aromatic ring is increased after the reduction while the C_β–C_γ distance is shortened, reflecting a more quinoidal character upon reduction. Both these trends and bond distances are in good agreement with the DFT-optimized geometry of $tpn^{\bullet-}$,[20] for which the calculations further confirm delocalization of the unpaired electron across the entire molecule.[20] This electronic structure underscores the potential of $tpn^{\bullet-}$ as a linker for high temperature molecule-based magnets and conductors.[32]

Although the N≡C bond lengths show only minor changes upon reduction, the FT-IR spectra reveal (Fig. S6, ESI†) a pronounced ~120–145 cm^{-1} red-shift of the $\nu_{C\equiv N}$ stretching from 2229 cm^{-1} in neutral tpn to 2104 cm^{-1} in $Li^+(tpn)^{\bullet-}(THF)_2$ and 2084 cm^{-1} in $Na^+(tpn)^{\bullet-}(THF)$ (Fig. S6, ESI†). This significant influence on the nitrile stretch provides strong spectroscopic evidence for radical anion formation, consistent with previous reports.[25]

Magnetic susceptibility measurements were carried out on polycrystalline powders of $Li^+(tpn)^{\bullet-}(THF)_2$ and $Na^+(tpn)^{\bullet-}(THF)$ (see ESI†). Fig. 4 shows the temperature dependence of the magnetic susceptibility (χ) of $Li^+(tpn)^{\bullet-}(THF)_2$ at 0.1 and 1 T plotted as a χT *vs.* T plot between 1.85 and 300 K. The χT product at 300 K is 0.372 cm^3 K mol^{-1} in good agreement with the Curie constant of

Table 1 Comparison of the bond lengths (Å) from neutral terephthalonitrile and radical terephthalonitrile in $Li^+(tpn)^{\bullet-}(THF)_2$ and $Na^+(tpn)^{\bullet-}(THF)$

	tpn at 100 K[31]	$Li(tpn)(THF)_2$ at 120 K	$Li(tpn)(THF)_2$ at 250 K	Na(tpn)(THF) at 120 K
N≡C	1.151(1)	1.156(4)–1.172(4)	1.160(4)	1.163(3)–1.164(3)
C_{CN}–C_α	1.434(1)	1.397(5)–1.408(5)	1.401(4)	1.400(3)–1.398(3)
C_α–C_β	1.392(1)–1.397(1)	1.419(5)–1.436(5)	1.398(5)–1.405(5)	1.421(3)–1.428(3)
C_β–C_γ	1.382(1)	1.358(4)–1.365(4)	1.350(4)	1.354(3)–1.360(3)
$C_\alpha\cdots C_\alpha$	2.748(1)	2.815(4)–2.827(4)	2.816(4)	2.820(3)

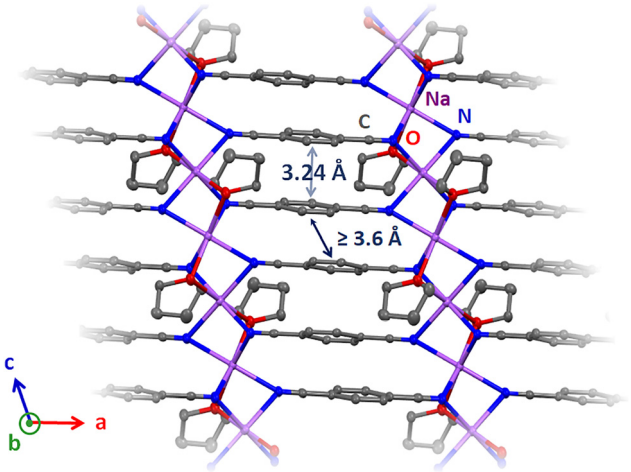

Fig. 3 Projection along the *b* axis of a portion of the 3-D coordination network of $Na^+(tpn)^{\bullet-}(THF)$ at 120 K. Thermal ellipsoids are depicted at a 50% probability level. Hydrogen atoms are omitted for clarity.

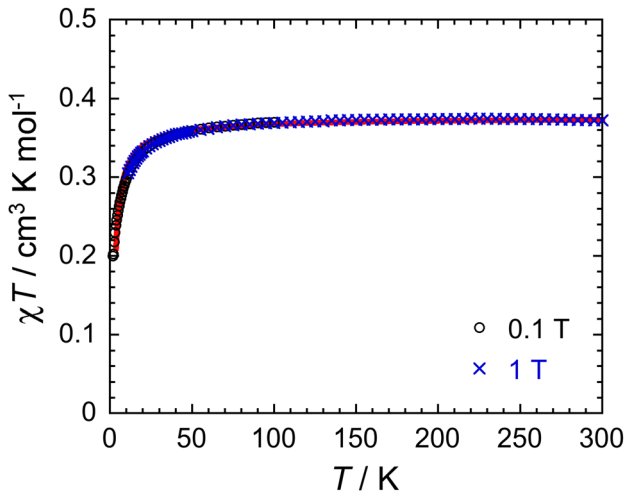

Fig. 4 Temperature (*T*) dependence of the χT product at 0.1 T (between 1.85 and 100 K) and 1 T (between 10 and 300 K) for $Li^+(tpn)^{\bullet-}(THF)_2$ (where $\chi = M/H$ is the molar magnetic susceptibility normalized per formula unit). The solid red line is the best fit of the experimental data to the regular $S = 1/2$ spin chain model described in the text.

0.375 $cm^3\ mol^{-1}$ K expected for an $S = 1/2$ radical species with a *g* factor of 2. As the temperature decreases, the presence of substantial antiferromagnetic interactions between radical molecules is highlighted by the marked decrease in the χT product below 50 K. Based on the crystal structures shown in Fig. 1 and 2, the strongest antiferromagnetic interactions between $(tpn)^{\bullet-}$ spins should be mediated by the Li cation along the $Li^+(tpn)^{\bullet-}$ chain. Accordingly, a regular chain of $S = 1/2$ quantum spins with a single magnetic interaction, *J*, between $(tpn)^{\bullet-}$ radical centers ($H = -2J\sum S_iS_{i+1}$) was used to model the magnetic susceptibility data. In 1964, Bonner and Fischer reported on this chain model and derived the analytical expression for the susceptibility,[33–35] which was used to fit the χT *vs.* *T* data shown in Fig. 4 (solid red line). This regular chain model is able to reproduce the experimental data well, with an estimated intrachain exchange coupling of $J/k_B = -1.39(6)$ K (with a *g* factor of 1.99(5)). In marked contrast to $Li^+(tpn)^{\bullet-}(THF)_2$, $Na^+(tpn)^{\bullet-}(THF)$ is completely diamagnetic below 300 K (with less than 0.15% of $S = 1/2$ Curie impurities – Fig. S11, ESI†), with an experimental diamagnetic susceptibility of $-0.64(5)\ 10^{-4}$ $cm^3\ mol^{-1}$, which compares well with the rough theoretical values derived from the molecular weight (MW; $-0.5 \times MW \times 10^{-6} = -1.1\ 10^{-4}$ $cm^3\ mol^{-1}$) or from Pascal's constants ($-1.3\ 10^{-4}$ $cm^3\ mol^{-1}$).[36] This magnetic behaviour results from strong π–π interactions between the neighbouring $tpn^{\bullet-}$ radicals,[24] forming diamagnetic radical pairs in the structure of $Na^+(tpn)^{\bullet-}(THF)$ ($d_{tpn-tpn} = 3.24$ Å; Fig. 3). This is also consistent with the EPR results. While the salts in solution display clear and expected EPR signals (Fig. S4, bottom, ESI†), the resonance for the solid $Na^+(tpn)^{\bullet-}(THF)$ is weak, revealing only a few percent of tpn radicals, in marked contrast with the solid $Li^+(tpn)^{\bullet-}(THF)_2$ under the same conditions (Fig. S4, top, ESI†).

In conclusion, the terephthalonitrile radical has been successfully synthesized, isolated and characterized as lithium and sodium THF-solvated salts. While neutral tpn has been widely used as an organic ligand, its radical form presents unique and compelling opportunities. These radical salts hold significant potential as (i) precursors for cross coupling reactions, (ii) versatile reductants and (iii) promising ligands for designing high-temperature molecule-based magnets or conductors. The latter application is particularly intriguing due to a remarkably large delocalization of its unpaired electron over the whole molecule, which could enhance the electronic and magnetic properties in these complexes.

This work was supported by the University of Bordeaux, the Région Nouvelle Aquitaine, the Centre National de la Recherche Scientifique (CNRS), the Institut Universitaire de France (IUF), Quantum Matter Bordeaux, the Association Française de Magnétisme Moléculaire (https://asso-am2.fr), the Academy of Finland (Projects 336456) and the China Scholarship Council (CSC) for the PhD funding of M. Suo. Alexandra Doussot is kindly acknowledged for support, and Apolline Morere for the graphical abstract.

Data availability

The data supporting this article have been included as part of the ESI.†

Conflicts of interest

There are no conflicts to declare.

Notes and references

1 L. S. Xie, G. Skorupskii and M. Dinca, *Chem. Rev.*, 2020, **120**, 8536–8580.
2 A. E. Thorarinsdottir and T. D. Harris, *Chem. Rev.*, 2020, **120**(16), 8716–8789.
3 P. Perlepe, I. Oyarzabal, I. A. Mailman, M. Yquel, M. Platunov, I. Dovgaliuk, M. Rouzières, P. Negrier, D. Mondieig, E. A. Suturina, M.-A. Dourges, S. Bonhommeau, R. A. Musgrave, K. S. Pedersen, D. Chernyshov, F. Wilhelm, A. Rogalev, C. Mathonière and R. Clérac, *Science*, 2020, **370**, 587–592.
4 I. Ratera and J. Veciana, *Chem. Soc. Rev.*, 2012, **41**, 303–349.
5 T. Faust and D. D'Alessandro, *RSC Adv.*, 2014, **4**, 17498–17512.
6 S. Demir, I.-R. Jeon, J. R. Long and T. D. Harris, *Coord. Chem. Rev.*, 2015, **289–290**, 149–176.
7 S. Kumar, Y. Kumar, S. Keshri and P. Mukhopadhyay, *Magnetochemistry*, 2016, **2**, 42.
8 A. Caneschi, D. Gatteschi, R. Sessoli and P. Rey, *Acc. Chem. Res.*, 1989, **22**, 392–398.
9 H. T. B. Pham, J. Y. Choi, M. Stodolka and J. Park, *Acc. Chem. Res.*, 2024, **57**, 580–589.
10 X. Ma, E. A. Suturina, S. De, P. Négrier, M. Rouzières, R. Clérac and P. Dechambenoit, *Angew. Chem., Int. Ed.*, 2018, **57**, 7841–7845.
11 X. Ma, E. A. Suturina, M. Platunov, M. Rouzières, F. Wilhelm, A. Rogalev, R. Clérac and P. Dechambenoit, *J. Am. Chem. Soc.*, 2019, **141**(19), 7721–7725.
12 X. Ma, E. A. Suturina, M. Rouzières, F. Wilhelm, A. Rogalev, R. Clérac and P. Dechambenoit, *Chem. Commun.*, 2020, **56**, 4906–4909.
13 J. M. Manriquez, G. T. Yee, R. S. McLean, A. J. Epstein and J. S. Miller, *Science*, 1991, **252**, 1415–1417.
14 R. C. Wheland and J. L. Gillson, *J. Am. Chem. Soc.*, 1976, **98**, 3916–3925.
15 S. Schmitt, M. Baumgarten, J. Simon and K. Hafner, *Angew. Chem., Int. Ed.*, 1998, **37**, 1077–1081.
16 K. Kano, K. Mori, B. Uno, M. I. Goto and T. Kubota, *J. Am. Chem. Soc.*, 1990, **112**, 8645–8649.
17 C. P. Andrieux, L. Gelis and J.-M. Savean, *J. Am. Chem. Soc.*, 1990, **112**, 786–791.
18 Q. Deng, S.-J. He, J. Pei, C. Fan, C. Li, B. Cao, Z.-H. Lu and J. Li, *Electrochem. Commun.*, 2017, **75**, 29–32.
19 E. V. Panteleevaa, G. Haufe and V. D. Shteingarts, *Synlett*, 2007, 1616–1618.
20 K. T. Workman, R. A. Firth and W. K. Gichuhi, *J. Phys. Chem. A*, 2023, **127**(1), 181–194.
21 B. Johnston, D. M. Loh and D. G. Nocera, *Angew. Chem., Int. Ed.*, 2023, **62**, e202312128.
22 E. V. Panteleeva, L. N. Shchegoleva, V. P. Vysotsky, L. M. Pokrovsky and V. D. Shteingarts, *Eur. J. Org. Chem.*, 2005, 2558–2565.
23 E. V. Panteleeva, M. Yu Lukyanova, L. M. Pokrovsky and V. D. Shteingarts, *Russ. Chem. Bull.*, 2007, **56**, 1110–1118.
24 R. Y. Peshkov, E. V. Panteleeva, W. Chunyan, E. V. Tretyakov and V. D. Shteingarts, *Beilstein J. Org. Chem.*, 2016, **12**, 1577–1584.
25 I. N. Juchnovski and I. G. Binev, *J. Mol. Struct.*, 1971, **7**, 490–494.
26 A. Carrington and P. F. Todd, *Mol. Phys.*, 1963, **6**, 161–168.
27 K. Nakamura, *Bull. Chem. Soc. Jap.*, 1967, **40**, 1019–1026.
28 L. Liu, J. A. DeGayner, L. Sun, D. Z. Zee and T. D. Harris, *Chem. Sci.*, 2019, **10**, 4652–4661.
29 N. M. Monezi and R. A. Ando, *Vib. Spectrosc.*, 2018, **99**, 67–72.
30 C. A. Hunter and J. K. M. Sanders, *J. Am. Chem. Soc.*, 1990, **112**, 5525–5534.
31 J. Yuan, Y. Wang, L. Li, S. Wang, X. Tang, H. Wang, M. Li, C. Zheng and R. Chen, *J. Phys. Chem. C*, 2020, **124**(18), 10129–10134.
32 H. Lv, D. Wu, X. Cui, X. Wu and J. Yang, *J. Phys. Chem. Lett.*, 2024, **15**, 9960–9967.
33 J. C. Bonner and M. E. Fisher, *Phys. Rev.*, 1964, **135**, A640–A658.
34 J. B. Torrance, Y. Tomkiewicz and B. D. Silverman, *Phys. Rev. B: Condens. Matter Mater. Phys.*, 1977, **15**, 4738–4749.
35 W. E. Estes, D. P. Gavel, W. E. Hatfield and D. J. Hodgson, *Inorg. Chem.*, 1978, **17**, 1415–1421.
36 G. A. Bain and J.-F. Berry, *J. Chem. Educ.*, 2008, **85**, 532–536.